Journal of Sound and Vibration (2002) **258**(2), 287–307
doi:10.1006/jsvi.5176, available online at http://www.idealibrary.com on IDEAL®

A SEMI-ANALYTICAL COUPLED FINITE ELEMENT FORMULATION FOR COMPOSITE SHELLS CONVEYING FLUIDS

J. Kochupillai, N. Ganesan and C. Padmanabhan

Machine Dynamics Laboratory, Department of Applied Mechanics, Indian Institute of Technology Madras, Madras 600 036*, India. E-mail: mouli@iitm.ac.in*

(*Received* 19 *September* 2001, *and in final form* 4 *March* 2002)

A coupled formulation based on the semi-analytical finite element technique is developed for composite shells conveying fluid. The structural finite element formulation is from Ramasamy and Ganesan (1998 *Computers and Structures* **70**, 363–376), while the fluid part is modelled by the characteristic wave equation. The fluid part is modelled using a velocity potential formulation and the dynamic pressure acting on the walls is derived from Bernoulli's equation. Impermeability and dynamic condition are imposed on the fluid–structure interface. The finite element equations for the composite shell conveying fluid are validated using available results in the literature. A detailed parametric study is carried out for various boundary conditions as well as for different length-to-radius and radius-to-thickness ratios.

1. INTRODUCTION

The dynamics of pipes conveying fluid has been studied extensively as can be seen from the review by Païdoussis and Li [1]. This review paper focuses more on the physical aspects of the problem than on mathematical formulations. Ramasamy and Ganesan [2] studied the vibration characteristics of fluid-filled shells with a constrained viscoelastic layer based on the Wilkins theory [3]. However, they did not consider fluid flow. Selman and Lakis [4] have developed a theory for the determination of the effects of flowing fluid on the vibration characteristics of an open anisotropic cylindrical shell submerged in a fluid and subjected simultaneously to an external and internal flow. They have used an analytical formulation to solve the fluid part. Olson and Jamaison [5] compared a general-purpose finite element program with analytical solution for elastic pipes conveying a fluid. Chang and Chiou [6] studied the natural frequencies and critical velocities of laminated circular cylindrical shells with fixed ends conveying fluids using a hybrid FE/analytical method. They used a Mindlin-type first order transverse shear deformable cylindrical shell theory for the structure and an analytical method for the fluid. For complex piping geometry, analytical techniques cannot be used. A number of investigators have proposed finite element formulations for fluid flow problems. For instance, Everstine [7] proposed a velocity potential formulation for a symmetric finite element solution of transient wave propagation problems, while Olson and Bathe [8] proposed a $\phi - u - p$ finite element formulation in order to eliminate the rigid body mode and enable the solution of static problems. Kock and Olson [9]

0022-460X/02/$35.00

introduced an Eulerian form of the non-linear velocity potential-density formulation and the significant feature is the derivation of the formulation from a single unified variational principle. Nitikitpaiboon and Bathe [10] extended the work of Olson and Bathe [8] by developing a non-linear $u-\phi-\rho-\lambda$ arbitrary Langrangian–Eulerian formulation in which both the velocity potential, ϕ, and the density ρ are employed. Their method takes into account the non-Eulerian nature of the finite element mesh for large boundary movements.

From the literature survey, it is found that, in general, most of the investigations reported deal with pipes conveying fluid, while there are only a few papers on shells. Most of the work deals with conventional materials. In addition, use of semi-analytical finite element formulation has not been attempted for composite materials. In the present study, a finite element formulation for a coupled fluid–structure interaction (FSI) problem for the case of a compressible fluid flow through composite shell has been attempted. The formulation is general in that it is applicable to any type of shell and is based on a potential-based finite element formulation for the fluid. Ramasamy and Ganesan [1] have used a pressure-based formulation, which is more suitable for stationary fluids. The present paper deals with the behaviour of different composite shells conveying fluids.

It is noted from the literature that pipe instability occurs predominantly in the bending mode (first circumferential mode, $n=1$). But for thin pipes conveying fluid, the instability can be of shell type. This is first reported by Païdoussis and Denise [11]. Hence in the present study, an analysis is carried out for composite shells conveying fluids for different boundary conditions of the shell, as well as different length-to-radius ratios ($l/a=1$, 4 and 25), different layer angles and radius-to-thickness ratios ($a/h=20$, 50, 100 and 200). Both divergence and coupled mode flutter instabilities can occur as seen from the literature. The main aim of this paper is to find out whether, it is possible to predict the type of instabilities that can occur in composite shells conveying fluids and establish a relation between the instability and the circumferential modes of the composite shell.

2. FINITE ELEMENT FORMULATION

2.1. STRUCTURE

Ramasamy and Ganesan [1] developed a general shell finite element for viscoelastic shells, based on the displacement field proposed by Wilkins *et al.* [3]. Figure 1 shows the schematic of the viscoelastic shell structure, consisting of a core viscoelastic layer sandwiched between two layers.

For the core layer, the displacement relations are

$$u^c = u_o + z\psi_s, \quad v^c = v_o + z\psi_\theta, \quad w^c = w_o, \tag{1}$$

where u, v, and w are the total displacements in the s, θ, and z directions.

For outer and inner facing, respectively, the displacement relations are

$$u^o, u^i = u_0 \pm hy_s + (z \pm h)f_s, \quad v^o, v^i = v_0 \pm hy_q + (z \pm h)f_q, \quad w^o, w^i = w_0. \tag{2}$$

Here "z" denotes the distance from the middle surface of the shell, "h" is half the core thickness and R is the radius of the circumferential direction. The θ direction variation is expressed in a Fourier series in the semi-analytical

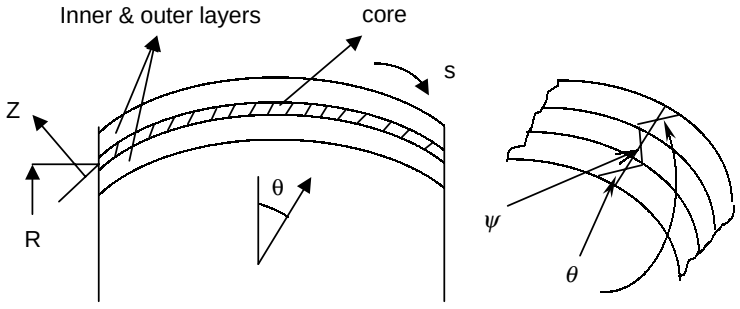

Figure 1. Viscoelastic structure.

formulation.

$$\begin{Bmatrix} u^o \\ v^o \\ w^o \\ \psi_s \\ \psi_\theta \\ \phi_s \\ \phi_\theta \end{Bmatrix} = \sum_{m=0}^{\infty} [\bar{\theta}_1] \begin{Bmatrix} u^{om1} \\ v^{om1} \\ w^{om1} \\ \psi_{sm1} \\ \psi_{\theta m1} \\ \phi_{sm1} \\ \phi_{\theta m1} \end{Bmatrix} + [\bar{\theta}_2] \begin{Bmatrix} u^{om2} \\ v^{om2} \\ w^{om2} \\ \psi_{sm2} \\ \psi_{\theta m2} \\ \phi_{sm2} \\ \phi_{\theta m2} \end{Bmatrix} \tag{3a}$$

where $[\bar{\theta}_1]$ and $[\bar{\theta}_2]$ are defined as follows

$$[\bar{\theta}_1] = \begin{bmatrix} c & & & & & & \\ & s & & & & & \\ & & c & & & & \\ & & & c & & & \\ & & & & s & & \\ & & & & & s & \\ & & & & & & c \end{bmatrix}, \quad [\bar{\theta}_2] = \begin{bmatrix} s & & & & & & \\ & c & & & & & \\ & & s & & & & \\ & & & s & & & \\ & & & & c & & \\ & & & & & c & \\ & & & & & & s \end{bmatrix}, \tag{3b}$$

where $c = \cos n\theta$, $s = \sin n\theta$.

In this case, a three-noded curved isoparametric ring element with seven degrees per node is derived using the semi-analytical method. The elemental displacement parameters are

$$u_e = \{u_{o1}, v_{o1}, w_{o1}, \psi_{s1}, \psi_{\theta 1}, \phi_{s1}, \phi_{\theta 1}, u_{o2}, v_{o2}, w_{o2}, \psi_{s2}, \ldots, w_{o3}, \psi_{s3}, \psi_{\theta 3}, \phi_{s3}, \phi_{\theta 3}\}, \tag{4}$$

where subscripts 1, 2 and 3 denote the three nodes. The strain–displacement relations, the shape functions and the elasticity matrix are given in reference [12]. Hence, the elemental stiffness and mass matrices are obtained from the following;

$$k_e = \int B^{\mathrm{T}} D B \, \mathrm{d}v, \quad m_e = \rho \int N^{\mathrm{T}} N \, \mathrm{d}v, \tag{5}$$

where k_e and m_e are the elemental stiffness and mass matrices and B is the strain matrix and N is the matrix of shape functions. Numerical integration using Gauss quadrature scheme is carried out for equation (5). If the same material is used for all the three layers, the above formulation will reduce to first order shear deformation theory and if curvature is in only one direction, this will become a cylinder.

2.2. FINITE ELEMENT FORMULATION OF THE FLUID DOMAIN (COMPRESSIBLE)

A semi-analytical, eight-noded, annular, isoparametric element is used for modelling the fluid domain. This is shown in Figure 2. The governing differential equation for the fluid region is popularly called the wave equation. It denotes the phenomenon in which the energy is propagated by waves and is applied to problems of sound propagation, sloshing of liquid and fluid–structure interaction. Its finite element expression has velocity potential as nodal degrees of freedom. The pressure in excess of hydrostatic pressure, p, is associated with the motion of the fluid. This pressure p is given by Bernoulli's equation.

The assumptions made are (1) the fluid flow is potential, (2) small deformations for the structure, i.e., linear, (3) flow is inviscid, irrotational and isentropic and fluid pressure is normal to the shell wall, (4) fluid is compressible and (5) there is no flow separation or cavitation.

The velocity potential should satisfy the wave equation and the associated boundary conditions shown below:

$$\nabla^2\phi - \frac{1}{c^2}\left(\frac{\partial}{\partial t} + U_x\frac{\partial}{\partial x}\right)^2\phi = 0. \tag{6}$$

In cylindrical co-ordinates, the wave equation is

$$\frac{1}{r}\frac{\partial}{\partial r}\left(r\frac{\partial\phi}{\partial r}\right) + \frac{1}{r^2}\frac{\partial^2\phi}{\partial\theta^2} + (1-M^2)\frac{\partial^2\phi}{\partial x^2} - \frac{1}{c^2}\frac{\partial^2\phi}{\partial t^2} - \frac{2U_x}{c^2}\frac{\partial^2\phi}{\partial x\partial t} = 0, \tag{7}$$

where ϕ is the velocity potential, c is the velocity of sound, U_x is the mean axial flow velocity of fluid and $M = U_x/c$ (Mach number). Therefore, we have

$$V_x = U_x + \frac{\partial\phi}{\partial x}, \quad V_\theta = \frac{1}{R}\frac{\partial\phi}{\partial\theta}, \quad V_r = \frac{\partial\phi}{\partial r}. \tag{8}$$

The radial velocity of the fluid must be equal to the instantaneous velocity of the shell. This will satisfy the impermeability or dynamic boundary conditions, which ensures contact between the shell and the fluid. That is,

$$V_r = \left.\frac{\partial\phi}{\partial r}\right|_{r=R} = \frac{\partial w}{\partial t} + U_x\frac{\partial w}{\partial x}. \tag{9}$$

The pressure acting on the shell surface is given by Bernoulli's equation for unsteady flow (Figure 3):

$$\frac{\partial\phi}{\partial t} + \frac{1}{2}V^2 + \frac{P}{\rho} = \frac{P_s}{\rho}, \tag{10}$$

where $V^2 = V_x^2 + V_\theta^2 + V_r^2$ and P_s is the stagnation pressure. Now P can be written as the sum of a mean pressure $\bar{P}$ and the perturbation pressure p:

$$P = \bar{P} + p. \tag{11}$$

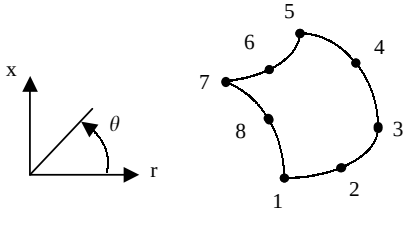

Figure 2. Cross-section of the annular fluid element.

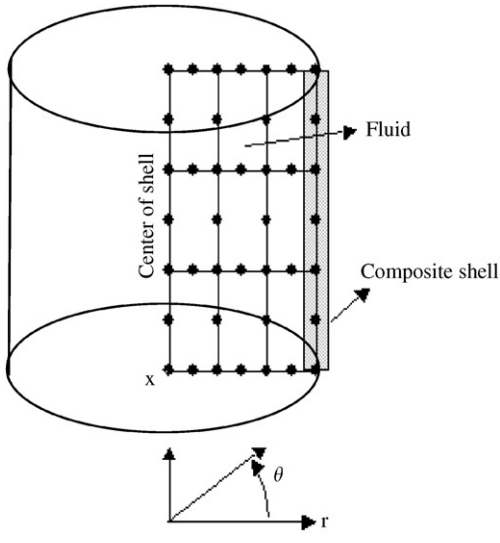

Figure 3. Discretization of the structure (3-noded line) and fluid (8-noded rectangle).

The non-linear terms in V^2 are neglected for small deformations, we get $V^2 \cong U_x^2 + 2U_x \partial\phi/\partial x$,

$$p = -\rho\left(\frac{\partial\phi}{\partial t} + U_x \frac{\partial\phi}{\partial x}\right). \tag{12}$$

A Galerkin weighted residual approach is used to formulate the finite element form of the governing wave equation in cylindrical co-ordinates. The result of the manipulations is:

$$\int_V N_f^{\mathrm{T}} \left(\nabla^2\phi - \frac{1}{c^2}\left(\frac{\partial}{\partial t} + U_x \frac{\partial}{\partial x}\right)^2 \phi\right) \mathrm{d}V = 0, \tag{13}$$

$$\int_S N_f^{\mathrm{T}} \nabla\phi \,\mathrm{d}S - \int_V \nabla N_f^{\mathrm{T}} \nabla\phi \,\mathrm{d}V - \frac{1}{c^2}\int_V N_f^{\mathrm{T}} \ddot{\phi} \,\mathrm{d}V - \frac{2U_x}{c^2}\int_V N_f^{\mathrm{T}} \frac{\partial^2\phi}{\partial x \partial t}\mathrm{d}V$$
$$- \frac{U_x^2}{c^2}\int_V N_f^{\mathrm{T}} \frac{\partial^2\phi}{\partial x^2}\mathrm{d}V = 0, \tag{14}$$

where N_f is the fluid shape functions given in reference [13]. The θ direction variation of ϕ is expressed in the form of a Fourier series. The first term of equation (14) is rewritten using the fluid–shell interface boundary condition of equation (9) as

$$\int_S N_f^{\mathrm{T}} \nabla\phi \,\mathrm{d}S = \int N_f^{\mathrm{T}} \bar{N}_s \,\mathrm{d}s\{\dot{U}_e\} + U_x \int N_f^{\mathrm{T}} \frac{\partial \bar{N}_s}{\partial x}\mathrm{d}S\{U_e\}, \tag{15}$$

where $\bar{N}_s$ is the w component of the shell shape function.

Similarly from equation (12), the pressure acting on the fluid–structure interface can be converted to the finite element equations,

$$\int_S \bar{N}_s^{\mathrm{T}} \rho_f \left(\frac{\partial\phi}{\partial t} + U_x \frac{\partial\phi}{\partial x}\right) \mathrm{d}S = \rho_f \int_S \bar{N}_s^{\mathrm{T}} N_f \,\mathrm{d}S\{\dot{\phi}_e\} + \rho_f U_x \int_S \bar{N}_s^{\mathrm{T}} \frac{\partial N_f}{\partial x}\mathrm{d}S\{\phi_e\}. \tag{16}$$

Now the complete fluid-structure finite element equation is

$$\begin{bmatrix} \mathbf{M}^{uu} & 0 \\ 0 & \mathbf{G}^{\phi\phi} \end{bmatrix} \begin{Bmatrix} \ddot{u} \\ \ddot{\phi} \end{Bmatrix} + \begin{bmatrix} \mathbf{0} & \mathbf{C}^{u\phi} \\ -\mathbf{C}^{\phi u} & -\mathbf{U}_x\mathbf{C}^{\phi\phi} \end{bmatrix} \begin{Bmatrix} \dot{u} \\ \dot{\phi} \end{Bmatrix} + \begin{bmatrix} \mathbf{K}^{uu} & \mathbf{U}_x\mathbf{K}^{u\phi} \\ -\mathbf{U}_x\mathbf{K}^{\phi u} & \mathbf{H}^{\phi\phi} - \mathbf{U}_x^2\mathbf{H}\mathbf{H}^{\phi\phi} \end{bmatrix} \begin{Bmatrix} u \\ \phi \end{Bmatrix} = 0, \tag{17}$$

where

$$\mathbf{m}_e = \rho \int_V \mathbf{N}^{\mathrm{T}}\mathbf{N}\,\mathrm{d}V, \quad \mathbf{M}^{uu} = \sum \mathbf{m}_e \quad \text{structural mass matrix},$$

$$\mathbf{G}_e^{\phi\phi} = \frac{1}{c^2}\int_V \mathbf{N}_f^{\mathrm{T}}\mathbf{N}_f\,\mathrm{d}V, \quad \mathbf{G}^{\phi\phi} = \sum \mathbf{G}_e^{\phi\phi}, \quad \text{compression energy of fluid},$$

$$\mathbf{C}_e^{u\phi} = \rho_f \int_S \bar{\mathbf{N}}_s^{\mathrm{T}}\mathbf{N}_f\,\mathrm{d}S, \quad \mathbf{C}^{u\phi} = \sum \mathbf{C}_e^{u\phi}, \quad \text{FSI coupling term},$$

$$\mathbf{C}_e^{\phi u} = \int_S \mathbf{N}_f^{\mathrm{T}}\bar{\mathbf{N}}_s\,\mathrm{d}S, \quad \mathbf{C}^{\phi u} = \sum \mathbf{C}_e^{\phi u}, \quad \text{FSI coupling term},$$

$$\mathbf{C}_e^{\phi\phi} = \frac{2}{c^2}\int_V \mathbf{N}_f^{\mathrm{T}}\frac{\partial \mathbf{N}_f}{\partial x}\mathrm{d}V, \quad \mathbf{C}^{\phi\phi} = \sum \mathbf{C}_e^{\phi\phi}, \quad \text{coriolis energy of fluid } U_x,$$

$$\mathbf{K}_e^{uu} = \int_V \mathbf{B}^{\mathrm{T}}\mathbf{D}\mathbf{B}\,\mathrm{d}V, \quad \mathbf{K}^{uu} = \sum \mathbf{K}_e^{uu}, \quad \text{structural stiffness matrix},$$

$$\mathbf{K}_e^{u\phi} = \rho_f \int_S \bar{\mathbf{N}}_s^{\mathrm{T}}\frac{\partial \mathbf{N}_f}{\partial x}\mathrm{d}S, \quad \mathbf{K}^{u\phi} = \sum \mathbf{K}_e^{u\phi}, \quad \text{stiffness coupling due to flow},$$

$$\mathbf{K}_e^{\phi u} = \int_S \mathbf{N}_f^{\mathrm{T}}\frac{\partial \bar{\mathbf{N}}_s}{\partial x}\mathrm{d}S, \quad \mathbf{K}^{\phi u} = \sum \mathbf{K}_e^{\phi u}, \quad \text{stiffness coupling due to flow},$$

$$\mathbf{H}_e^{\phi\phi} = \int_V \nabla\mathbf{N}_f^{\mathrm{T}}\nabla\mathbf{N}_f\,\mathrm{d}V, \quad \mathbf{H}^{\phi\phi} = \sum \mathbf{H}_e^{\phi\phi}, \quad \text{kinetic energy of fluid},$$

$$\mathbf{H}\mathbf{H}_e^{\phi\phi} = \frac{1}{c^2}\int_V \frac{\partial \mathbf{N}_f^{\mathrm{T}}}{\partial x}\frac{\partial \mathbf{N}_f}{\partial x}\mathrm{d}V, \quad \mathbf{H}\mathbf{H}^{\phi\phi} = \sum \mathbf{H}\mathbf{H}_e^{\phi\phi}, \quad \text{centrifugal energy of fluid, } U_x^2,$$

Rewriting the above equation in state-space form by letting $\{d\} = \{u\ \ \phi\ \ \dot{u}\ \ \dot{\phi}\}^{\mathrm{T}}$:

$$\lambda \begin{bmatrix} -\mathbf{C}\mathbf{C} & -\mathbf{M}\mathbf{M} \\ \mathbf{M}\mathbf{M} & \mathbf{0} \end{bmatrix} \{d\} = \begin{bmatrix} \mathbf{K}\mathbf{K} & \mathbf{0} \\ \mathbf{0} & \mathbf{M}\mathbf{M} \end{bmatrix} \{d\}, \tag{18}$$

where

$$\mathbf{M}\mathbf{M} = \begin{bmatrix} \mathbf{M}^{uu} & \mathbf{0} \\ \mathbf{0} & \mathbf{G}^{\phi\phi} \end{bmatrix}, \quad \mathbf{K}\mathbf{K} = \begin{bmatrix} \mathbf{K}^{uu} & U_x\mathbf{K}^{u\phi} \\ -U_x\mathbf{K}^{\phi u} & \mathbf{H}^{\phi\phi} - U_x^2\mathbf{H}\mathbf{H}^{\phi\phi} \end{bmatrix},$$

$$\mathbf{C}\mathbf{C} = \begin{bmatrix} \mathbf{0} & \mathbf{C}^{u\phi} \\ -\mathbf{C}^{\phi u} & -U_x\mathbf{C}^{\phi\phi} \end{bmatrix}.$$

The shell and fluid motion are coupled by the off diagonal terms of the damping and stiffness matrices. For stationary fluids, the coupling in stiffness vanishes. The equation is converted into state-space form equation (18) and the resulting eigenvalues are then

determined using LAPACK routine, DGEGV [14]. A sample finite element discretisation is shown in Figure 3.

2.3. FINITE ELEMENT FORMULATION OF THE FLUID DOMAIN (INCOMPRESSIBLE)

In this case, the fluid is assumed as incompressible, all other assumptions hold well as in the previous case. Here, the velocity potential should satisfy the Laplace equation and the boundary conditions:

$$\nabla^2 \phi = 0. \tag{19}$$

In cylindrical co-ordinates, the Laplace equation is

$$\frac{1}{r}\frac{\partial}{\partial r}\left(r\frac{\partial \phi}{\partial r}\right) + \frac{1}{r^2}\frac{\partial^2 \phi}{\partial \theta^2} + \frac{\partial^2 \phi}{\partial x^2} = 0, \tag{20}$$

where ϕ is the velocity potential. As above, a similar Galerkin weighted residual approach is used to formulate the finite element form of the governing Laplace equation in cylindrical co-ordinates. The matrix equation is shown below:

$$\begin{bmatrix} \mathbf{M}^{uu} & \mathbf{0} \\ \mathbf{0} & \mathbf{0} \end{bmatrix} \begin{Bmatrix} \ddot{u} \\ \ddot{\phi} \end{Bmatrix} + \begin{bmatrix} \mathbf{0} & \mathbf{C}^{u\phi} \\ -\mathbf{C}^{\phi u} & \mathbf{0} \end{bmatrix} \begin{Bmatrix} \dot{u} \\ \dot{\phi} \end{Bmatrix} + \begin{bmatrix} \mathbf{K}^{uu} & U_x\mathbf{K}^{u\phi} \\ -U_x\mathbf{K}^{\phi u} & \mathbf{H}^{\phi\phi} \end{bmatrix} \begin{Bmatrix} u \\ \phi \end{Bmatrix} = 0. \tag{21}$$

Now we can condense the fluid equation as below:

$$-\mathbf{C}^{\phi u}\dot{\boldsymbol{u}} - U_x\mathbf{K}^{\phi u}u + \mathbf{H}^{\phi\phi}\phi = 0, \tag{22}$$

$$\phi = \mathbf{H}^{\phi\phi-1}\mathbf{C}^{\phi u}\dot{\boldsymbol{u}} + U_x\mathbf{H}^{\phi\phi-1}\mathbf{K}^{\phi u}u, \tag{23}$$

$$\dot{\phi} = \mathbf{H}^{\phi\phi-1}\mathbf{C}^{\phi u}\ddot{\boldsymbol{u}} + U_x\mathbf{H}^{\phi\phi-1}\mathbf{K}^{\phi u}\dot{\boldsymbol{u}}. \tag{24}$$

Substituting ϕ and $\dot{\phi}$ into the structural equation, we get

$$\begin{aligned}[\mathbf{M}^{uu} + \mathbf{C}^{u\phi}\mathbf{H}^{\phi\phi-1}\mathbf{C}^{\phi u}]\,\ddot{\boldsymbol{u}} + U_x[\mathbf{C}^{u\phi}\mathbf{H}^{\phi\phi-1}\mathbf{K}^{\phi u} + \mathbf{K}^{u\phi}\mathbf{H}^{\phi\phi-1}\mathbf{C}^{\phi u}]\dot{\boldsymbol{u}} \\ + [\mathbf{K}^{uu} + U_x^2\mathbf{K}^{u\phi}\mathbf{H}^{\phi\phi-1}\mathbf{K}^{\phi u}]u = 0.\end{aligned} \tag{25}$$

This can be written in the state-space form by letting $\{d\} = \{\, u \quad \dot{\boldsymbol{u}} \,\}^{\mathrm{T}}$:

$$\lambda \begin{bmatrix} -\mathbf{CC} & -\mathbf{MM} \\ \mathbf{MM} & \mathbf{0} \end{bmatrix} \{d\} = \begin{bmatrix} \mathbf{KK} & \mathbf{0} \\ \mathbf{0} & \mathbf{MM} \end{bmatrix} \{d\}, \tag{26}$$

where $\mathbf{MM} = [\mathbf{M}^{uu} + \mathbf{C}^{u\phi}\mathbf{H}^{\phi\phi-1}\mathbf{C}^{\phi u}]$, $\mathbf{CC} = U_x[\mathbf{C}^{u\phi}\mathbf{H}^{\phi\phi-1}\mathbf{K}^{\phi u} + \mathbf{K}^{u\phi}\mathbf{H}^{\phi\phi-1}\mathbf{C}^{\phi u}]$, and $\mathbf{KK} = [\mathbf{K}^{uu} + U_x^2\mathbf{K}^{u\phi}\mathbf{H}^{\phi\phi-1}\mathbf{K}^{\phi u}]$.

In this case, an added mass term, an added damping term (similar to coriolis effect) due to potential formulation and an added stiffness term (similar to centrifugal effect) due to stiffening by the pressure acting on the walls are present.

3. RESULTS AND DISCUSSION

A semi-analytical finite element formulation for compressible and incompressible flow through composite shells is formulated. Using the state-space approach, the combined equation for the structure and the fluid is solved for the compressible flow model (equations (17) and (18)). For incompressible flow model, equation (25) is written in the state-space form, i.e., equation (26) and solved. An eigenvalue analysis of composite shells conveying fluids at different flow velocities is carried out. For each circumferential mode

(denoted by n), the associated axial modes (denoted by m) are computed. The results obtained from the present formulation are validated with results quoted in the literature. In addition, the results are obtained using both compressible and incompressible flow models for different boundary conditions. These are compared for an l/a ratio of 1 and an a/h ratio of 100. Subsequently, using the incompressible flow model, a detailed parametric study is attempted for different boundary conditions, l/a ratios, a/h ratios and different layer angles. To find out the effect of element size on the eigenvalues, the results of two, four and eight elements in the radial direction and eight, 16 and 20 elements along the length and its combinations are compared. It is found out that for the present formulation, two elements in the radial direction and eight elements in the longitudinal direction will give accurate results.

3.1. VALIDATION

Païdoussis [15] has studied the static and dynamic instabilities of pipes conveying fluids. He derived the governing differential equation for the coupled fluid structure system considering the pipe as a beam. In order to validate the present formulation, the results for circumferential mode $n = 1$, which corresponds to the beam mode and for material properties of mild steel are used. For the non-dimensional parameter $\beta = 0{\cdot}8$, which represents the ratio of the fluid mass to the sum of structural and the fluid masses, the comparison is shown in Figure 4. The graph shows the dimensionless flow velocity u versus the dimensionless frequency ω/ω_0, where ω is the frequency of the structure in rad/s, ω_0 is $\sqrt{(EI/(m+M)L^4)}$ and u is $\sqrt{(EI/ML^2)}U_x$ where U_x is the flow velocity in m/s, m is the mass per unit length of pipe (kg/m), M is the mass per unit length of fluid (kg/m) and L is the length of pipe in m.

Figure 4 shows excellent agreement for the results of present formulation with that of Païdoussis [15] (Figure 4). For composite shells the results of Chang and Chiou [6] is compared. Chang and Chiou [6] have studied the natural frequencies and critical velocities of laminated circular cylindrical shells with fixed–fixed ends conveying fluids. They used

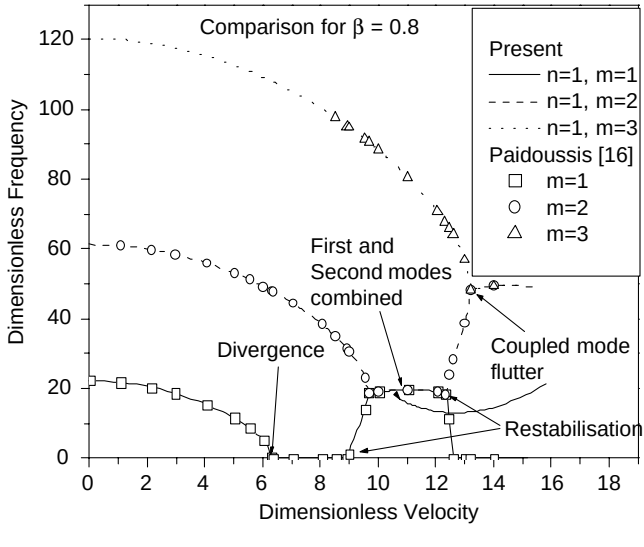

Figure 4. Comparison with the results of Païdoussis [15] and the present for $\beta = 0{\cdot}8$.

TABLE 1

Comparison of present formulation with Chang and Chiou [6]

$l/a = 25$, $h/a = 0{\cdot}05$, $\alpha = 0$, CC, $\rho_f = 10{\cdot}67808$			
Circumferential mode	Axial mode	Chang and Chiou critical velocity	Present critical velocity
1	1	3·55	4·05
1	2	4·35	4·39
2	1	2·75	3·02
2	2	2·85	3·04 (coupled mode flutter)
3	1	3·43	3·31
3	2	3·47	3·41

Mindlin-type first order transverse shear deformation cylindrical shell theory for the analysis. Equations of motion are derived by Hamilton's principle. Fluid pressure acting on the wall is obtained through the continuity condition and the assumption of the ideal flow. Hence, the finite element code developed for incompressible flow is validated with the results from Chang and Chiou [6] as shown in Figure 5. The results are obtained for a cylindrical pipe with $l/a = 25$, $h/a = 0{\cdot}05$ and α (angle of ply) $= 0$. Critical velocities for circumferential modes 1–3 are compared in Table 1. The values in the table indicate good agreement, but the present method generally predicts the values on the higher side. It is to be noted that the non-dimensional frequencies for the zero flow case reported by Chang and Chiou [6] do not exactly agree with results published in the literature [15]. The deviations are probably due to their numerical implementation using the Bessel function. The typical dimensionless material constants used by Chang and Chiou [6] for a single layer, in its material principal axes are as follows: dimensionless velocity is U_x/U_0 where $U_0 = \sqrt{E_0/\rho_s}$, dimensionless frequency $\Omega = \omega/\omega_0 \times 100$ where $\omega_0 = U_0/a$, ω is the real natural frequency, a is the radius of the shell, ρ_s is the density of the shell material and $E_1/E_0 = 21$, $E_2/E_0 = E_3/E_0 = 1{\cdot}7$, $G_{12}/E_0 = G_{13}/E_0 = 0{\cdot}65$, $G_{23}/E_0 = 0{\cdot}639$, where E_1, E_2, E_3 are Young's moduli and (G_{12}, G_{13}, G_{23}) is the vector of shear moduli for the composite shell. In the present study, the non-dimensional velocity is taken as $U_0 = E_1/\rho$ (Figure 5).

3.2. COMPARISON OF COMPRESSIBLE AND INCOMPRESSIBLE FLOW MODELS

First, a comparison between the compressible and the incompressible flow models is carried out to study the effect of compressibility in the dynamic characteristics of the composite shell conveying fluids. It is to be mentioned here that in order to use the potential formulation for compressible flow, small density changes are assumed. A composite shell of radius 10 cm, length 10 cm and thickness 1 mm with clamped–clamped boundary condition is modelled and analyzed. Figure 6 shows the comparison of compressible and incompressible flow models for composites graphite/epoxy and kevlar/epoxy for circumferential modes corresponding to their respective minimum critical velocities. As expected, the real eigenvalues decrease as the flow velocity increases and at a particular point the real eigenvalue vanishes at point A. This velocity is called the critical velocity. If the flow velocity is increased further, the real eigenvalue reappears (B) and it coalesces with the next higher axial mode real eigenvalue (C) and moves together to the next higher mode (C–D). The first mode eigenvalue separates after some time, decreases

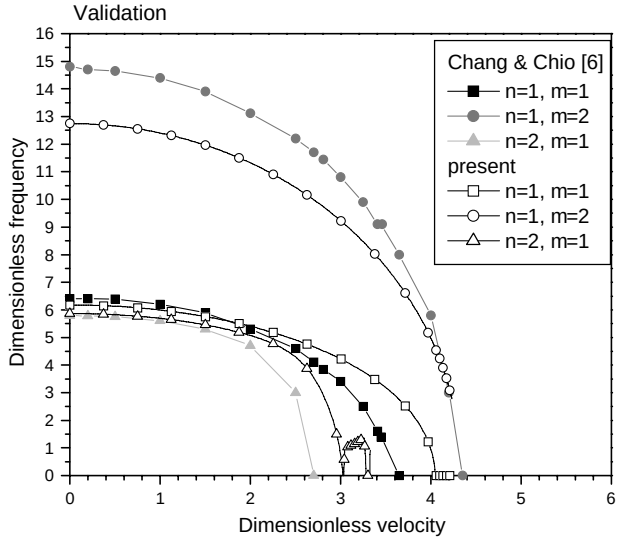

Figure 5. Validation of the present study with that of Chang and Chiou [6].

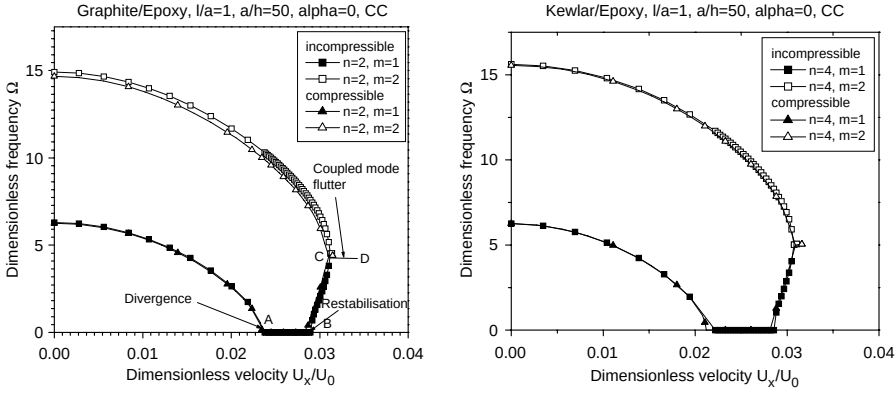

Figure 6. Comparison between compressible and incompressible flow models for circumferential modes corresponding to lowest critical velocity.

and then vanishes. In the region where both the real eigenvalues of axial modes 1 and 2 are the same (C–D), coupled mode flutter-type instability occurs. It is observed that for the compressible flow model, buckling velocity or the critical velocity is lower than that of the incompressible flow model. It is also found that for the circumferential mode at which buckling occurs earlier, the effect of compressibility is minimal. That is the effect of compressibility decreases as the circumferential mode number increases and has least difference near about the circumferential mode at which the lowest critical velocity is predicted. Again for higher axial modes, there is considerable difference in the two models. This study is repeated for other boundary conditions such as clamped–free (CF) and simply supported (SS). Results obtained for different boundary conditions show similar trends. To find out the effect of compressibility with respect to the circumferential modes, a study is carried out for the first 10 circumferential modes. Figure 6 shows the result of

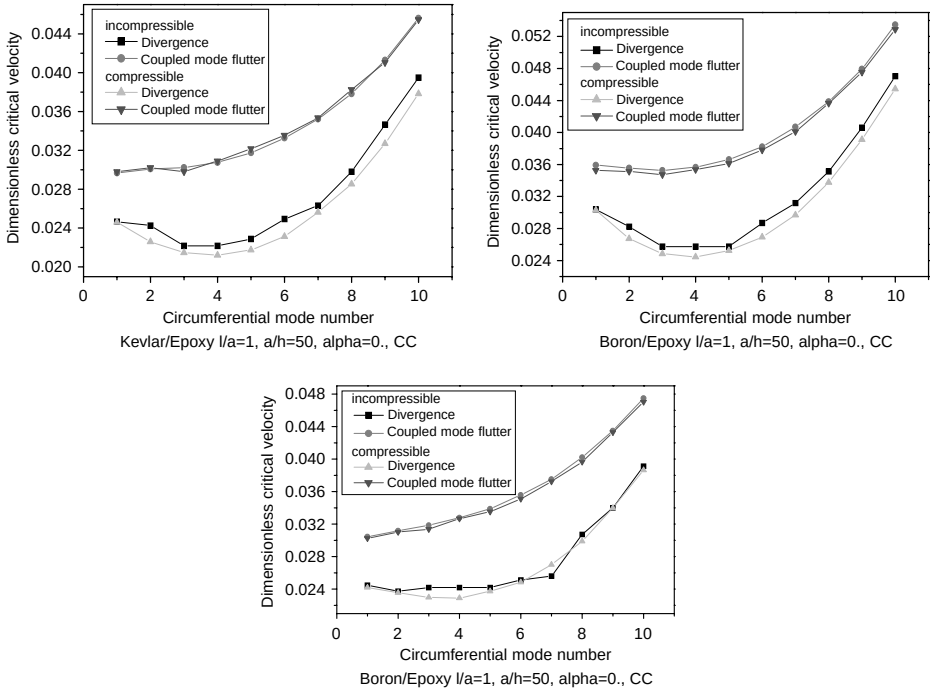

Figure 7. Comparison of critical velocities and coupled mode flutter points for circumferential modes 1–10.

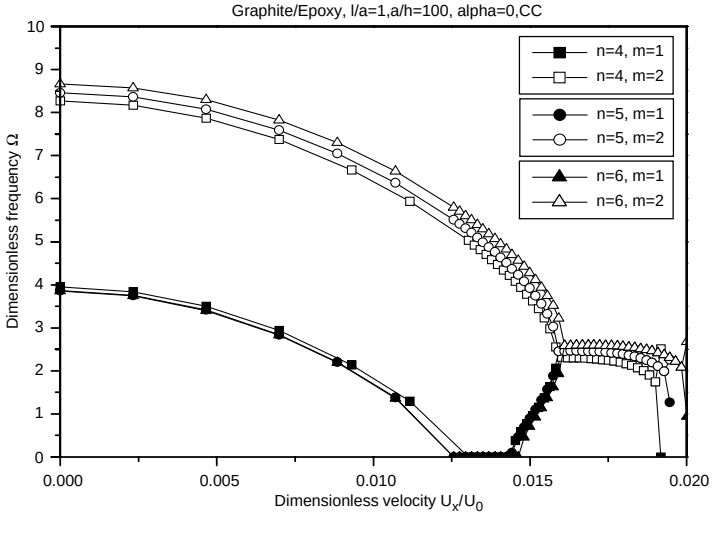

Figure 8. Dimensionless frequency versus Dimensionless velocity for graphite/epoxy for circumferntial mode ($n = 4, 5, 6$) where 5 is the critical buckling mode and for axial modes 1 and 2.

this study. Figure 7 gives the critical velocity and coupled mode flutter obtained by the compressible flow model and by the incompressible flow model versus the circumferential mode numbers. It is seen from Figure 7 that the critical velocity differs with respect to the

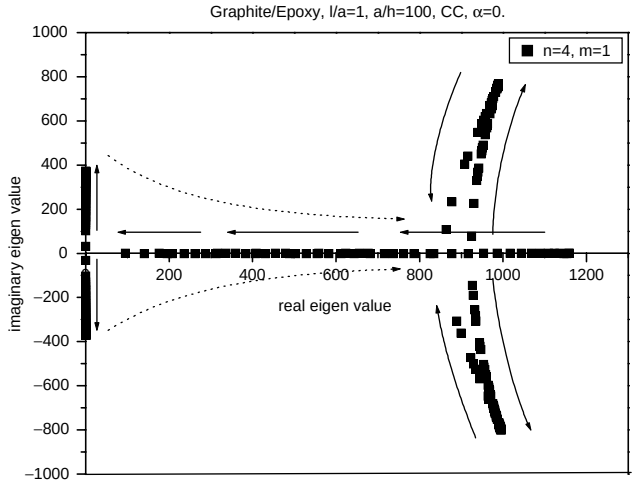

Figure 9. Real eigenvalue versus imaginary eigenvalue.

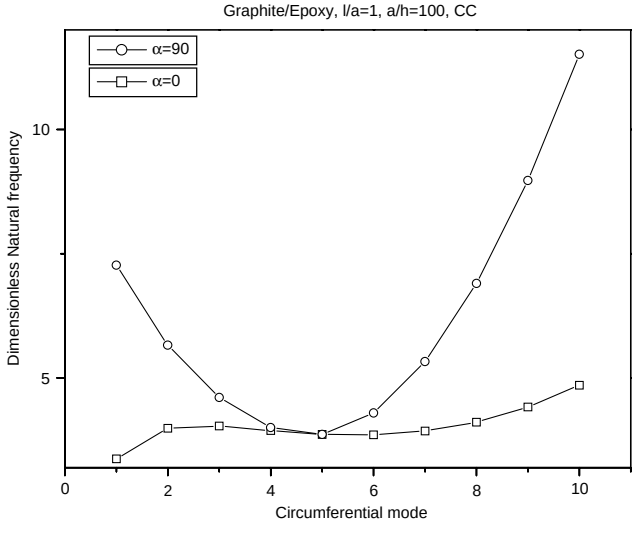

Figure 10. Dimensionless natural frequency versus circumferential mode.

circumferential mode and it is found that the lowest critical velocity corresponds to the circumferential mode number 4 for $l/a = 1$, $a/h = 50$ and $\alpha = 0$ for both compressible and incompressible flow models. For this particular l/a ratio, the critical circumferential mode number is 4 for graphite/epoxy, kevlar/epoxy and boron epoxy.

3.3. BUCKLING STUDIES ON CLAMPED–CLAMPED SHELL

Characterizing the influence of the aspect ratio (l/a) and slenderness ratio (a/h) on the critical velocity is the main aim of the present study. In addition, another major aim of the

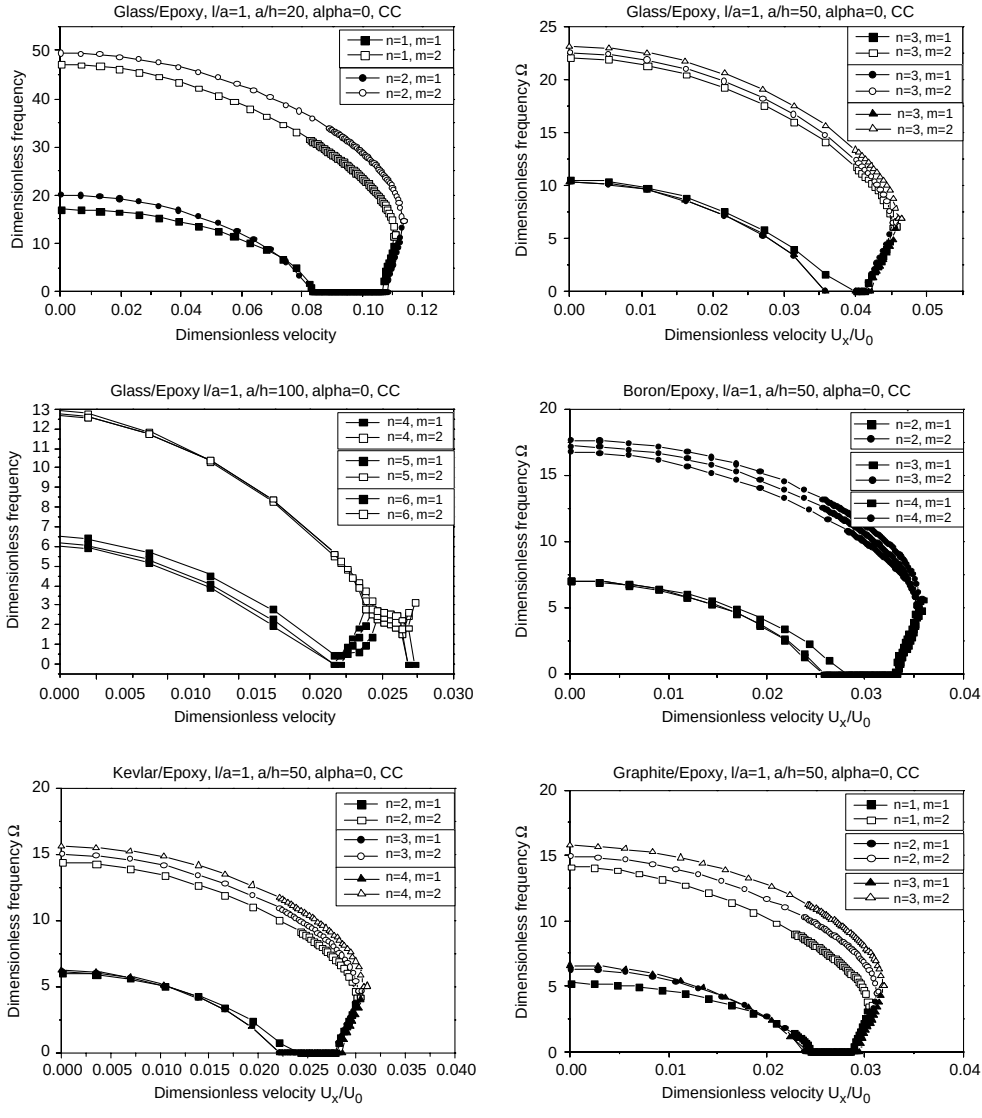

Figure 11. Dimensionless frequency versus dimensionless velocity for composites, glass/epoxy, boron/epoxy, kewlar/epoxy, and graphite/epoxy for clamped–clamped boundary condition for different l/a and h/a ratios.

present study is to correlate the critical velocity and the natural frequency characteristics of the composite shell. This is done with a view to develop design guidelines. To start with, a composite (graphite/epoxy) shell of radius 10 cm, length 10 cm and thickness 1 mm with clamped–clamped boundary condition is studied. The non-dimensional velocity versus non-dimensional frequency is shown in Figure 8. Ten circumferential modes ($n = 1-10$) and the corresponding two axial modes ($m = 1, 2$) are computed using the incompressible flow model from which the one corresponding to the lowest critical velocity and two adjacent to that mode are shown in Figure 8. Here also the real eigenvalues decrease as the flow velocity increases. The real eigenvalue vanishes at critical velocities (divergence-type

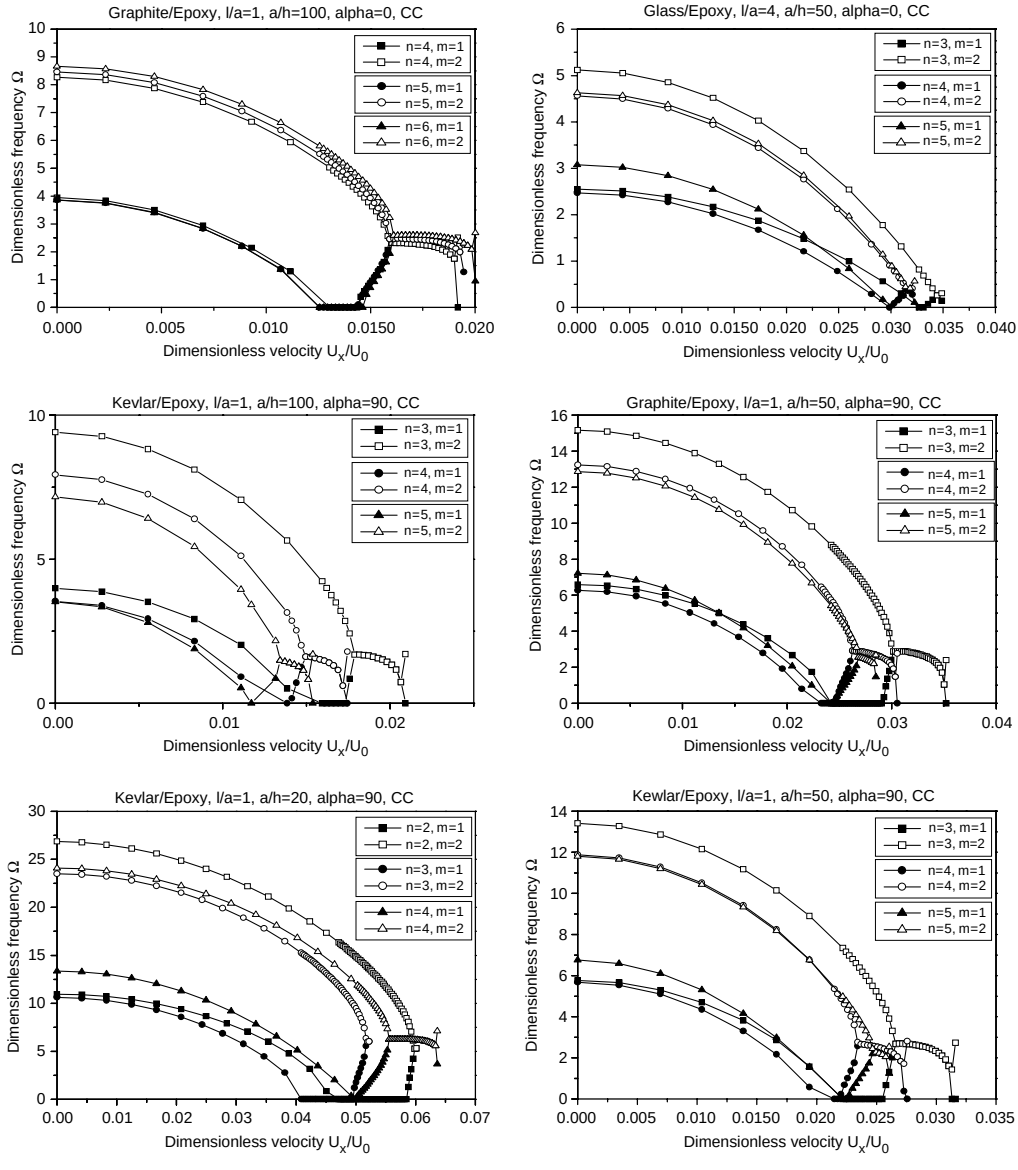

Figure 11. (*continued*)

buckling) and reappears as the flow is further increased. The coupled mode flutter-type instability occurs from the point where the first and the second axial mode eigenvalues coalesce. The imaginary part also gives an indication of the type of buckling mode, i.e., either divergence or coupled mode flutter. Until the critical flow velocity is reached, the imaginary eigenvalues are either zero or very near zero and for velocities above the critical velocity, the imaginary eigenvalues becomes larger. This is shown in Figure 9. This means that the system is not stable. From Figure 8, it is observed that the buckling occurs first for the circumferential mode 5 and this corresponds to the lowest natural frequency of the fluid-filled shell as shown in Figure 10.

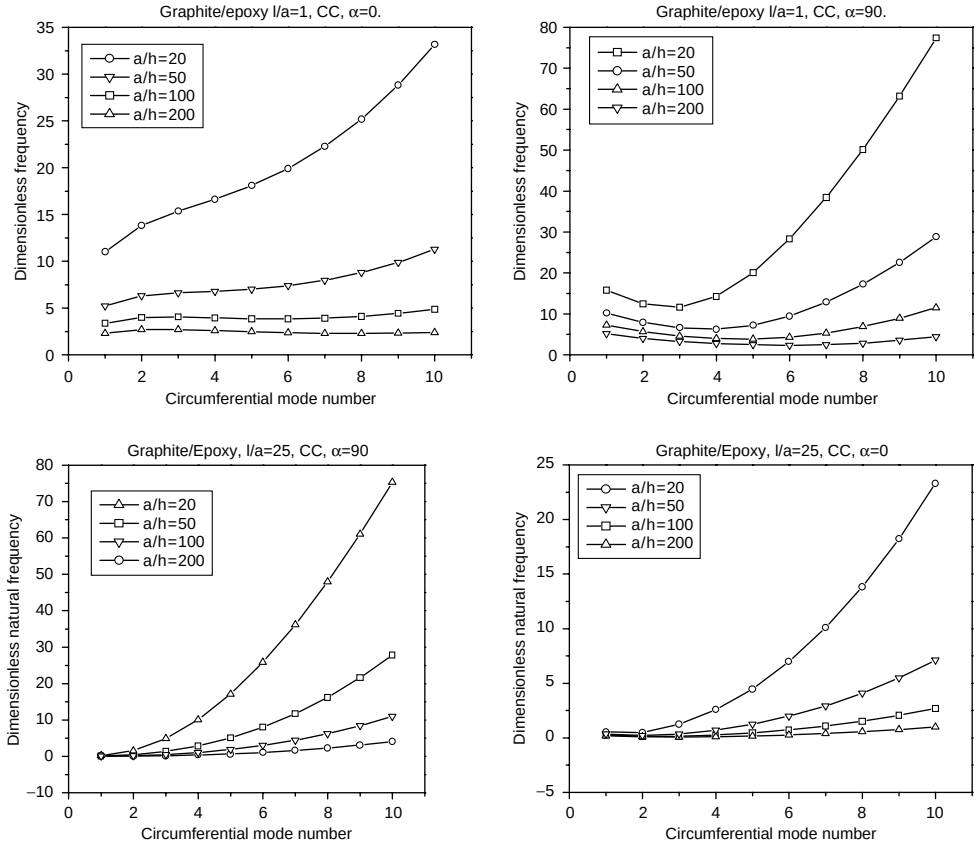

Figure 12. Dimensionless natural frequency versus Circumferential mode number.

Even though the main aim of the present study is to understand the divergence type of buckling behaviour of composite shells, which usually occurs before coupled mode flutter, an attempt is made to link the circumferential mode corresponding to the lowest critical velocity to that of the circumferential mode having the lowest natural frequency of the fluid-filled shell. Subsequent to the above study, a typical detailed study has been made on a shell with clamped–clamped boundary condition, aspect ratios (1, 4, 25) and layer angles (0, 45, 90). In present study, the influence of flow velocities on the natural frequency characteristics of composite clamped–clamped shells of length-to-radius ratios 1, 4, 25 has been carried out for typical radius-to-thickness ratios (20, 50, 100, 200). The variation of dimensionless flow velocities with dimensionless frequency has been shown in Figure 11. It is found from the graph that for large aspect ratios ($l/a = 25$) buckling, in general, occurs near the first circumferential mode ($n = 1$). This agrees with the buckling of pipelines in bending mode. In general, the buckling of composite shells is a complicated phenomenon and depending upon the type of loading, boundary condition and parameters of the shell, it may occur at different circumferential modes. Divergence buckling may perhaps be categorized as static buckling. Hence, an attempt is being made to explain the behaviour from the natural frequencies of the shell. To this end, the frequency characteristics of different shells were obtained (without flow consideration). The lowest frequencies of different shells with different aspect ratios occur at different circumferential modes. In

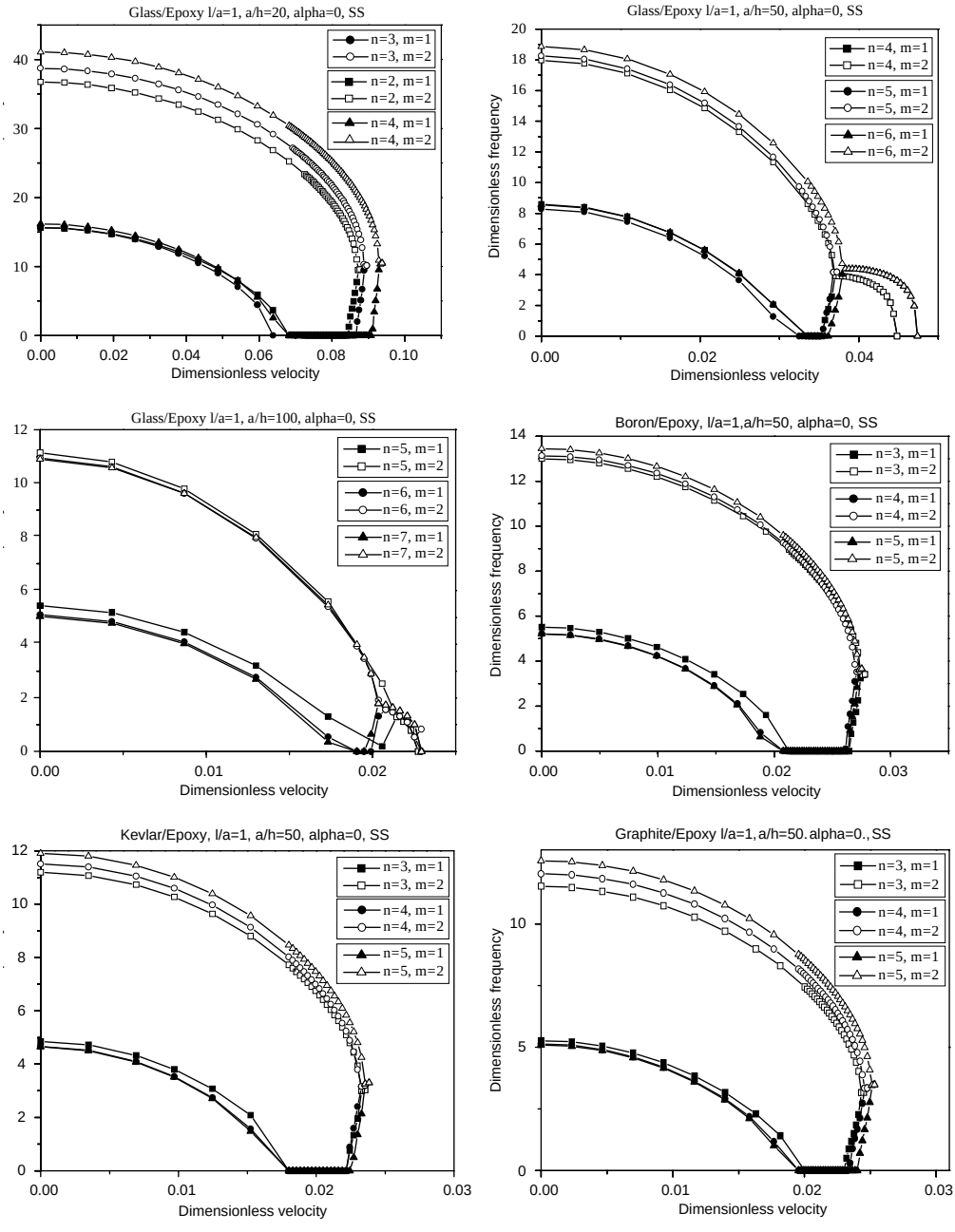

Figure 13. Dimensionless frequency versus dimensionless velocity for composites, glass/epoxy, boron/epoxy, kevlar/epoxy, and graphite/epoxy for simply supported boundary condition for different l/a and h/a ratios.

addition, a detailed study was made on the buckling behaviour of different shells for all the circumferential modes. From this study, the circumferential mode pertaining to the lowest critical velocity was identified and on comparing with Figure 12, it is

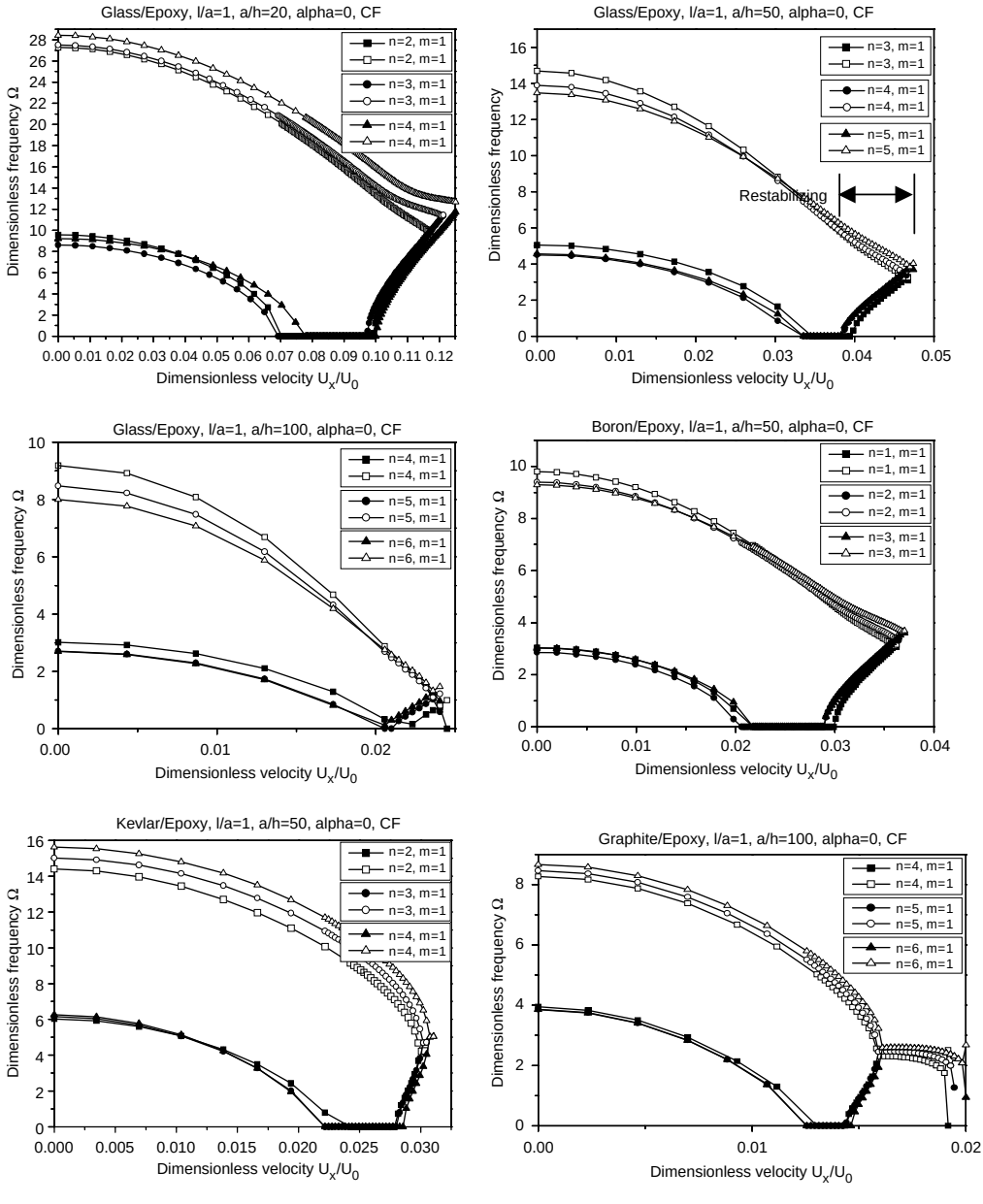

Figure 14. Dimensionless frequency versus dimensionless velocity for composites, glass/epoxy, boron/epoxy, kevlar/epoxy, and graphite/epoxy for clamped–free boundary condition for different l/a and h/a ratios and layer angles.

found that there is a clear correlation between the circumferential buckling modes of composite shells conveying fluids and the circumferential mode at which the lowest natural frequency occurs for the fluid-filled composite shell, especially for $\alpha = 90$ as shown in Figure 12.

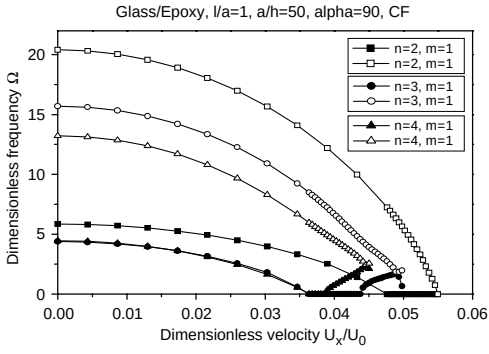

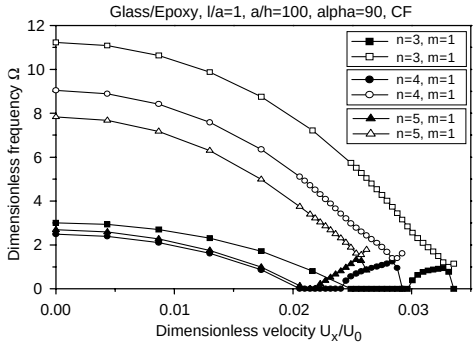

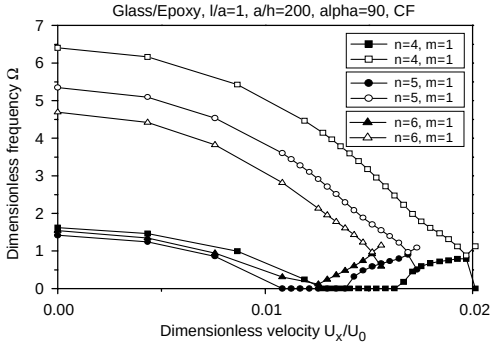

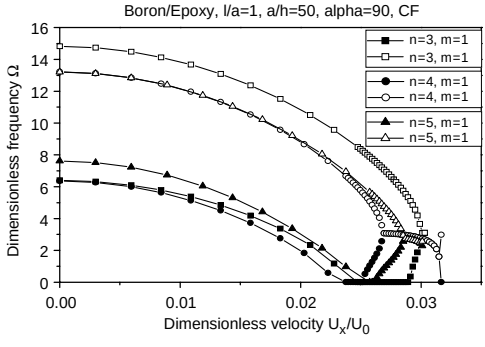

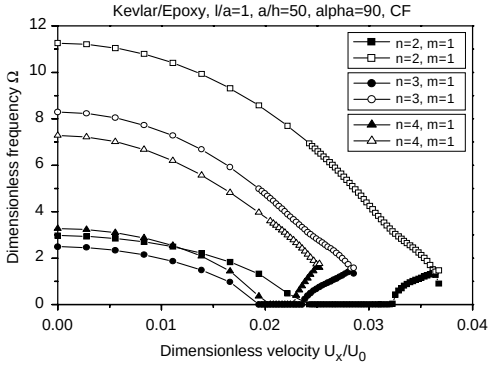

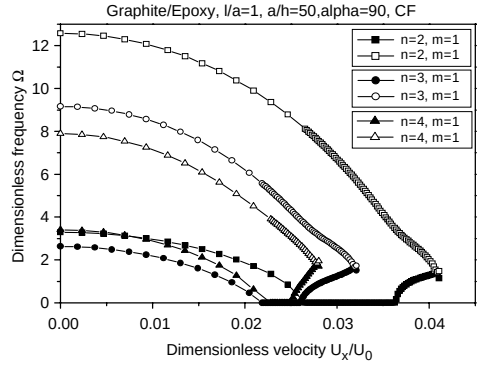

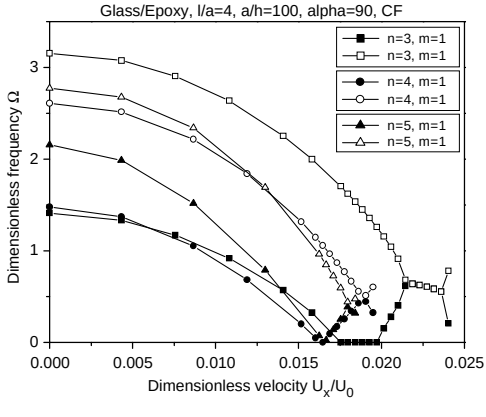

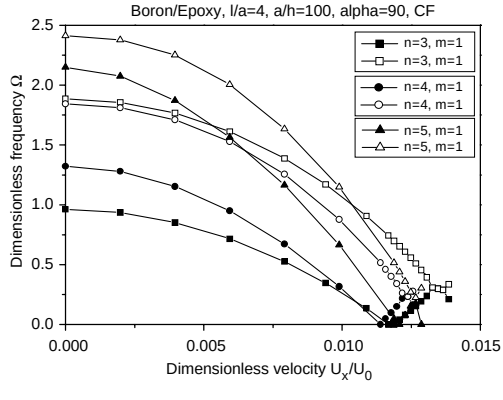

Figure 14. (*continued*)

TABLE 2

Comparison of circumferential mode having the lowest natural frequency for the fluid-filled composite shell and that of circumferential modes at which buckling occurs first

Boundary condition	Case	Circumferential mode at which the lowest natural frequency occurs		Circumferential mode at which the buckling occurs	
		$\alpha = 0$	$\alpha = 90$	$\alpha = 0$	$\alpha = 90$
CF	Graphite/epoxy, $l/a = 1$, $a/h = 20$	1	3	1	3
	Graphite/epoxy, $l/a = 1$, $a/h = 50$	1	4	1	4
	Graphite/epoxy, $l/a = 1$, $a/h = 100$	1	5	5	5
	Graphite/epoxy, $l/a = 1$, $a/h = 200$	8	6	6	6
	Graphite/epoxy, $l/a = 4$, $a/h = 20$	8	6	3	2
	Graphite/epoxy, $l/a = 4$, $a/h = 50$	4	2	4	3
	Graphite/epoxy, $l/a = 4$, $a/h = 100$	5	3	6	4
	Graphite/epoxy, $l/a = 4$, $a/h = 200$	8	4	7	5
	Graphite/epoxy, $l/a = 25$, $a/h = 20$	2	1	2	1
	Graphite/epoxy, $l/a = 25$, $a/h = 50$	2	1	2	1
	Graphite/epoxy, $l/a = 25$, $a/h = 100$	2	1	3	2
	Graphite/epoxy, $l/a = 25$, $a/h = 200$	3	2	4	2
SS	Graphite/epoxy, $l/a = 1$, $a/h = 20$	1	3	3	3
	Graphite/epoxy, $l/a = 1$, $a/h = 50$	1	4	4	4
	Graphite/epoxy, $l/a = 1$, $a/h = 100$	1	5	6/7	4/5
	Graphite/epoxy, $l/a = 1$, $a/h = 200$	9	6	5	6
	Graphite/epoxy, $l/a = 4$, $a/h = 20$	3	2	3	2
	Graphite/epoxy, $l/a = 4$, $a/h = 50$	4	3	4	2
	Graphite/epoxy, $l/a = 4$, $a/h = 100$	5	3	5	3
	Graphite/epoxy, $l/a = 4$, $a/h = 200$	6	3	6	3
	Graphite/epoxy, $l/a = 25$, $a/h = 20$	2	2	2	2
	Graphite/epoxy, $l/a = 25$, $a/h = 50$	2	2	2	2
	Graphite/epoxy, $l/a = 25$, $a/h = 100$	2	2	2	1
	Graphite/epoxy, $l/a = 25$, $a/h = 200$	2	1	3/4	1
CC	Graphite/epoxy, $l/a = 1$, $a/h = 20$	3	2	3	2
	Graphite/epoxy, $l/a = 1$, $a/h = 50$	4	3	3/4	3
	Graphite/epoxy, $l/a = 1$, $a/h = 100$	6	4	5/6	4
	Graphite/epoxy, $l/a = 1$, $a/h = 200$	7	4	7/8	4
	Graphite/epoxy, $l/a = 4$, $a/h = 20$	3	1	3	2
	Graphite/epoxy, $l/a = 4$, $a/h = 50$	3	2	4	2
	Graphite/epoxy, $l/a = 4$, $a/h = 200$	4	2	5/6	2
	Graphite/epoxy, $l/a = 25$, $a/h = 20$	1	2	4	2
	Graphite/epoxy, $l/a = 25$, $a/h = 50$	1	1	2	2
	Graphite/epoxy, $l/a = 25$, $a/h = 100$	2	1	2	2
	Graphite/epoxy, $l/a = 25$, $a/h = 200$	2	1	2	1

3.4. BUCKLING STUDIES ON SIMPLY SUPPORTED AND CLAMPED–FREE COMPOSITE SHELL

A detailed study has been carried out on composite shells with simply supported boundary condition and aspect ratios (1, 4, and 25). The present study examines the influence of flow velocities on the natural frequency characteristics of composite simply supported shells of length-to-radius ratios 1, 4 and 25 with typical radius-to-thickness ratios (20,50,100 and 200). To start with the frequency characteristics of different shells were obtained (with out flow consideration). Variation of dimensionless

flow velocities with dimensionless frequency has been shown in Figure 13. Here also, it is seen that there is a good correlation between the circumferential mode at which the lowest critical velocity occurs and the circumferential mode at which the shell has got the lowest frequency. A similar study is carried out for clamped–free boundary condition to study the correlation between the circumferential mode at which lowest critical velocity of the composite shell occurs and the circumferential mode corresponding to the lowest frequency of the system (Figure 14). It is found that the above correlation is applicable to all boundary conditions in general. This may be due to the fact that the stiffness of the shell for that particular circumferential mode which buckles earlier is the least. Table 2 summarizes the fact that the circumferential mode at which lowest critical velocity occurs and the circumferential mode corresponding to the lowest frequency of the system show good correlation for all the boundary conditions investigated.

4. CONCLUSIONS

A semi-analytical coupled finite element formulation is developed for general shells conveying fluids. More complicated geometry can be easily modelled using the present formulation. A comparison between compressible and incompressible flow models indicates that compressibility has little effect on circumferential modes close to those buckling modes corresponding to the lowest critical velocity. The finite element formulation works well for the classical boundary conditions, i.e., clamped–clamped, clamped–free and simply supported. For very short shells, the buckling mode is the bending mode and as the length of the shell increases, the buckling mode shifts to higher circumferential modes and eventually returns to the bending mode. In general, the circumferential mode at which the lowest critical velocity occurs corresponds to the circumferential mode at which the lowest frequency of the system occurs. This is true for all aspect ratios and boundary conditions studied. Hence, the frequency characteristics can be used, to identify the circumferential mode at which the lowest critical velocity will occur, for design purposes. In the case of clamped–free boundary condition, the system stabilizes after divergence and then goes to couple mode flutter type of instability. This is shown in Figure 14. In certain cases, different axial modes come within the same frequency range thus showing a high degree of coupling. This could also lead to coupled mode flutter type of instability and will be investigated in future. More complex piping geometry will also be investigated shortly.

REFERENCES

1. R. Ramasamy and N. Ganesan 1998 *Computers and Structures* **70**, 363–376. Finite element analysis of fluid filled isotropic cylindrical shells with constrained viscoelastic damping.
2. M. P. Païdoussis and G. X. Li 1993 *Journal of Fluid and Structures* **7**, 137–204. Pipes conveying fluid: A model dynamical problem.
3. D. J. Wilkins Jr, C. W. Bert and D. M. Egle *Journal of Sound and Vibration* **13**, 211–228. Free vibrations of orthotropic sandwich conical shells with various boundary conditions.
4. A. Selman and A. A. Lakis 1997 *Journal of Fluids and Structures* **11**, 111–134. Vibration analysis of anisotropic open cylindrical shells subjected to flowing fluid.
5. L. G. Olson and D. Jamison 1997 *Journal of Fluids and Structures* **11**, 207–222. Application of a general purpose finite element method to elastic pipes conveying fluid.
6. Jeng-Shian Chang and Wen-Jiann Chiou 1995 *Computers and Structures* **57**, 929–939. Natural frequencies and critical velocities of fixed-fixed laminated circular cylindrical shells conveying fluids.

7. G. C. Everstine 1981 *Journal of Sound and Vibration* **79**, 157–160. A symmetric potential formulation for fluid-structure interaction. Letter to the Editor.
8. L. G. Olson and K. J. Bathe 1985 *Computers and Structures* **21**, 21–32. Analysis of fluid-structure interaction. A direct symmetric coupled formulation based on the fluid velocity potential.
9. E. Kock and L. G. Olson 1991 *International Journal of Numerical Methods in Engineering* **31**, 463–491. Fluid Structure interaction analysis by the finite element method. A variational approach.
10. C. Nitikitpaiboon and K. J. Bathe 1993 *Computers and Structures* **47**, 877–891. An arbitrary Lagrangian-Eulerian velocity potential formulation for fluid structure interaction.
11. M. P. Paidousis and J. P. Denise 1972 *Journal of Sound and Vibration* **20**, 9–26. Flutter of thin cylindrical shells conveying fluid.
12. T. C. Ramesh and N. Ganesan 1991 *Computers and Structures* **46**, 751–758. Vibration and damping characteristics of cylindrical shells with a constrained damping layer.
13. C. T. F. Ross 1994 *Pressure Vessels Under External Pressure: Statics and Dynamics*. London: Elsevier Applied Science.
14. G. H. Golub and C. F. Van Loan 1996 *Matrix Computations*. Baltimore: Johns Hopkins University Press; third edition.
15. M. P. Païdoussis 1975 *Journal of Mechanical Engineering Science* **17**, 19–25. Flutter of conservative systems of pipes conveying incompressible fluid.